JOURNAL OF CATALYSIS **162,** 1–9 (1996)
ARTICLE NO. 0254

Reduction of NO over Partially Reduced Metal-Loaded CeO_2–ZrO_2 Solid Solutions

G. Ranga Rao,* P. Fornasiero,† R. Di Monte,‡ J. Kašpar,†,[1] G. Vlaic,† G. Balducci,† S. Meriani,‡ G. Gubitosa,§ A. Cremona,§ and M. Graziani†

*International Centre for Science and High Technology, APH Grignano, 34100 Trieste, Italy; †Dipartimento di Scienze Chimiche, Università di Trieste, Via Giorgieri 1, 34127 Trieste, Italy; ‡Dipartimento di Ingegneria dei Materiali e Chimica Applicata, Università di Trieste, Via Valerio 2, 34127 Trieste, Italy; and §Magneti Marelli D.S.S., Viale Carlo Emanuele II 150, 10078 Venaria Reale, Turin, Italy

Received January 4, 1995; revised December 13, 1995; accepted March 30, 1996

CeO_2–ZrO_2 solid solutions supported with Rh and Pt are investigated as catalysts for reduction of NO by CO. The incorporation of ZrO_2 into the CeO_2 framework strongly promotes the reduction of Ce^{4+} in the bulk of the support. The effects of the reduction temperature are investigated and it is shown that when bulk oxygen vacancies are formed in the reduced CeO_2–ZrO_2 solid solution, NO is efficiently decomposed on the support to give N_2O and N_2. The presence of bulk oxygen vacancies is indicated as the driving force for NO dissociation, suggesting their indirect participation in the catalytic cycle.

INTRODUCTION

In recent years much research has been focused on cerium oxide based transition metal catalysts because of their applications in different processes, particularly in the catalytic treatment of automotive exhausts. CeO_2 is indeed extensively added as a promoter to the current three-way catalyst (TWC). Several functions are attributed to this promoter (1, 2), namely (i) stabilization of metal dispersion and its alumina support; (ii) promotion of water gas shift and steam reforming reactions, and (iii) oxygen storage and release capacities under respectively fuel-lean and fuel-rich conditions due to the redox couple $2CeO_2 \rightleftharpoons Ce_2O_3 + 1/2O_2$. The last point is of relevant technological importance since high oxygen storage capacity (OSC) allows one to enlarge the operating air/fuel window and thus it increases the overall efficiency of TWCs in the working conditions.

To increase the catalytic efficiency of TWCs during a cold start, close-coupled locations of the converter are usually employed. Therefore, in the driving conditions the operating temperature may easily exceed 1200 K, requiring high thermal stability of the catalyst. Upon ageing at such high temperatures, deactivation of the catalyst may occur due to sintering of metal particles, formation of irreducible rhodium species, and collapse of the Al_2O_3 surface area. In addition, the OSC of the CeO_2 strongly decreases upon thermal ageing, due to the growth of CeO_2 crystallites and/or formation of $CeAlO_3$ (3). Addition of ZrO_2 to the washcoat improves the thermal stability of the catalyst by hindering the sintering of the CeO_2 particles (4). This suggests that a close interaction between CeO_2 and ZrO_2 may thermally stabilize the CeO_2. Therefore, incorporation of CeO_2 into a solid solution with ZrO_2 might provide a suitable way to improve the thermal resistance of the material due to the ceramic nature of these systems. Furthermore, in the solid solution, the undesirable decline of the OSC due to fixation of the Ce^{4+}/Ce^{3+} redox couple in the 3+ state ($CeAlO_3$, $Ce_2(SO_4)_3$) should be limited. On the basis of these considerations we decided to study CeO_2–ZrO_2 mixed oxides as supports for noble metal catalysts. Our initial investigation evidenced a remarkable promotion of the reducibility of Rh-loaded CeO_2–ZrO_2 solid solutions in comparison to Rh/CeO_2. The OSC as measured by oxygen uptake was strongly enhanced in comparison to Rh/CeO_2 catalysts, independently of the surface area, and this was attributed to the participation of lattice oxygen in the redox processes (5).

This observation prompted us to investigate the behavior of metal-loaded CeO_2–ZrO_2 solid solutions as catalysts for the reduction of NO by CO to give N_2 and CO_2. This reaction is a key step in the catalytic conversion of automotive exhausts since it is believed that NO is removed by its reaction with CO over rhodium. Rhodium promotes the above reaction due to its ability to efficiently dissociate NO in comparison to other platinum group metals. NO dissociation is believed to be the rate-determining step of the reaction, at least at low temperatures (6). Here we report evidence for NO dissociation occurring over reduced ceria-containing catalysts, suggesting a new role of both the metal and ceria in the TWCs under transient conditions. A preliminary report of the present results appeared recently (7).

[1] E-mail: kaspar@dschsun1.univ.trieste.it; Fax: 39-40-6763903.

0021-9517/96 $18.00

EXPERIMENTAL

CeO_2–ZrO_2 solid solutions were prepared by firing mixtures of the oxides (CeO_2, Medolla, ZrO_2, Harshaw 102) at 1873 K for 1 h and then cooling to room temperature (r.t.) at a rate of 10 K min^{-1}. Single point BET areas were measured by N_2 adsorption at 77 K on a Micromeritics surface area analyzer. All the samples showed surface areas in the range 1–2 m^2 g^{-1}. Powder X-ray diffraction patterns were collected on a Siemens Kristalloflex Mod.F Instrument (Ni-filtered Cu$K\alpha$). Supports were impregnated with $RhCl_3 \cdot 3H_2O$ or $Na_2PtCl_6 \cdot nH_2O$ to incipient wetness and afterwards the catalysts were dried at 393 K overnight. This procedure was repeated 5–7 times until the nominal metal loading of 0.5 wt% was attained. The catalysts were then calcined at 723 K for 4 h.

Catalytic experiments were carried out in differential conditions using a U-shaped quartz microreactor (NO (2%) in He, total flow 15 ml min^{-1} or NO (1%) and CO (3%) in He, total flow 30 ml min^{-1}, GHSV = 12500–50000 h^{-1}). Typically 0.04–0.08 g of the catalyst (granules 75–350 μm) were loaded between two layers of granular quartz which acted as a preheater. Reaction temperature was monitored by means of a thermocouple located in the catalyst bed. The effluents of the reactor (NO, N_2, N_2O, CO, and CO_2) were analyzed by an on-line Hewlett–Packard 5890 II gaschromatograph equipped with a thermal conductivity detector (TCD). Presence of O_2 in the effluents could be detected at the ppm level. The separation of the gaseous mixture, including O_2, could be achieved by employing Hayesep A and Porapak Q columns. Research grade purity gas mixtures (>99.997%) were employed without further purification. GLC analysis showed the presence of traces of N_2O and N_2 in the feed mixture which have been taken into account in the conversion measurements. Temperature programmed oxidation (TPO) experiments using NO as oxidant were carried out in a flow of NO (2% in He, 7 ml min^{-1}) at a heating rate of 2 K min^{-1} using the same equipment as employed for the catalytic measurements. Temperature programmed reduction (TPR) experiments were carried out as previously described (5), using a conventional system equipped with a TCD. A flow of H_2 (5%) in Ar (25 ml min^{-1}) and a heating rate of 10 K min^{-1} were employed. Magnetic susceptibility was measured with a Metronique MS02 SQUID magnetometer at 294 K with a static magnetic field of 12.5 kOe. Weighed samples were treated *in situ* with H_2 or NO in a quartz sample holder and sealed under an inert atmosphere. The susceptibility was corrected for the diamagnetic contribution of the sample holder. Estimation of the degree of reduction was performed by using the value $\chi(Ce_2O_3 \text{ at } 294 \text{ K}) = 1.06 \times 10^{-5}$ emu g^{-1} (8).

X-ray absorption near edge structure (XANES) measurements were carried out at the EXAFS-I station on the DCl storage ring (energy 1.85 GeV, current 300 mV) at LURE (Orsay, France). The spectra were collected in the transmission mode, in the range of energies 5670–5790 eV by steps of 0.3 eV. A channel-cut Si 331 monochromator was employed and ionization chambers were filled with air. Absence of any contribution to the spectrum of photons due to the third harmonic was accurately checked. Preedge background was linearly fitted in the region 5680–5710 eV, and its contribution was then subtracted from the experimental spectrum. All spectra were normalized to 1 at the energy of 5790 eV. For the measurements at the Ce L_{III} edge, a thin film (5–7 mg cm^{-2}) of the catalyst was deposited onto a graphite holder from an acetone suspension, which was then inserted in an *in situ* XANES cell. The *in situ* XANES experiments were carried out using the same conditions as employed for the NO–CO and NO reactions.

RESULTS AND DISCUSSION

TPR Characterization

Ceria-zirconia solid solutions exist in three different phases, namely monoclinic, tetragonal, and cubic (9). The metastable tetragonal phase is easily formed by the ceramic method in a wide compositional interval (10–50 mol% of CeO_2), and it is fairly stable at ordinary temperatures (10). Above 50 mol% of CeO_2, the cubic phase is formed (10c). At 50% of CeO_2, the cubic phase may be prepared and easily transforms by thermal treatment into the tetragonal phase (11). We showed that the kinetics of the redox processes are favored in the cubic samples, compared to the tetragonal ones (5). Moreover, upon increasing the ZrO_2 content in the cubic phase, the temperature of the peak associated with support reduction decreases while the reverse is observed for the tetragonal phase. On the basis of these observations we have chosen to investigate as a catalyst for the reduction of NO by CO, the $M/Ce_{0.6}Zr_{0.4}O_2$ (M = Rh, Pt) samples. This support composition has the highest ZrO_2 content compatible with a stable cubic phase.

The role of ZrO_2 in promoting the oxygen exchange properties of the CeO_2-containing supports is exemplified by the TPR profiles reported in Fig. 1. In the profile of both the Rh- and Pt-loaded $Ce_{0.6}Zr_{0.4}O_2$ (surface area ≈ 1 m^2 g^{-1}) there appears a strong reduction peak at about 700 K (hereinafter indicated as LT, low temperature peak). Reduction of Rh_2O_3 supported on CeO_2 usually occurs at about 370 K (2). Therefore, keeping in consideration the magnitude of the peak at 700 K, we attribute the LT peak to the reduction of the solid solution in the bulk. At variance with this, PtO_2 is reduced at 500 K (2) which suggests that in this case the reduction of the metal oxide and of the support occur almost concurrently.

By contrast, low surface area (≈ 1 m^2 g^{-1}) $Ce_{0.6}Zr_{0.4}O_2$, Rh/CeO_2, and CeO_2 do not show any peak below 950 K attributable to support reduction (Fig. 1, traces 3–5). The absence of the LT feature in $Ce_{0.6}Zr_{0.4}O_2$ is attributed to the very low surface area of the sample which does not

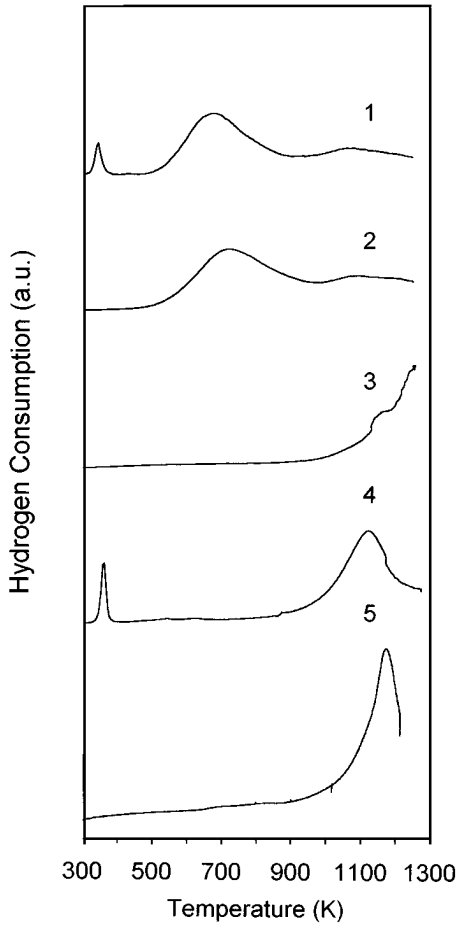

FIG. 1. Temperature programmed reduction profiles of (1) 0.5% $Rh/Ce_{0.6}Zr_{0.4}O_2$, (2) 0.5% $Pt/Ce_{0.6}Zr_{0.4}O_2$, (3) $Ce_{0.6}Zr_{0.4}O_2$, (4) 0.5% Rh/CeO_2, (5) CeO_2.

allow an efficient H_2 activation. In the presence of the supported metal, which spills hydrogen over to the support, the efficiency of the reduction process is enhanced. The reduction kinetics are then limited by the oxygen mobility in the bulk which is higher in the solid solution than in pure CeO_2 (5). The lower oxygen mobility in the bulk can account for the lack of the LT feature in both the CeO_2 and Rh/CeO_2 samples (Fig. 1, traces 4–5). In accordance with this interpretation, we found a strong dependence of the kinetics of both reduction and oxidation processes upon the structural properties of the $Rh/Ce_mZr_{1-m}O_2$ ($m = 0.1$–1) solid solutions (5).

The ability of the M/CeO_2–ZrO_2 system to undergo reduction at relatively low temperatures is important, in view of the previous observations that reductive pretreatment strongly enhances the catalytic activity of a TWC in transient conditions (12). Similarly, enhancement of activity after a reduction in H_2 have been observed in CO oxidation (13) and CO_2 hydrogenation (14). The rate enhancement in transient conditions was associated with the formation of oxygen vacancies located at the periphery of the metal particles (14). We have therefore focused our attention on the effects of reduction on the catalytic properties of the Pt and $Rh/Ce_{0.6}Zr_{0.4}O_2$ catalysts. For the sake of comparison some selected experiments obtained on Rh/CeO_2 are also reported.

NO Reduction by CO and NO Conversion over Reduced Catalysts: Effects of Reduction Temperature

The activity of the catalysts reduced at 473 and 673 K was investigated in a flow reactor. Typically, the catalysts were reduced in H_2 at the chosen temperature for 2 h, deareated in a flow of He and then aged in the reaction mixture for 6–8 h before the steady state activities were measured. Apparent activation energies were measured over the aged catalysts in the course of run-up cycles (heating rate 1 K min^{-1}, from 473 to 600 K). The steady state activities and the apparent activation energies for the NO and CO conversions are summarized in Table 1.

There is an interesting difference in the apparent activation energies observed over the $Rh/Ce_{0.6}Zr_{0.4}O_2$ catalyst reduced at 673 K and the other systems investigated: Rh/CeO_2 reduced at 473 and 673 K, $Rh/Ce_{0.6}Zr_{0.4}O_2$ reduced at 473 K. Two apparent activation energies respectively above and below approximately 500 K were obtained in the first case, while in all the other cases, the whole range of temperatures investigated is characterized by a single activation energy. The change of the activation energies upon reduction at 473 and 673 K is illustrated in Fig. 2. It is worth noting the quite low apparent activation energy for NO conversion below 500 K observed after a reduction at 673 K on the $Rh/Ce_{0.6}Zr_{0.4}O_2$ catalyst (Table 1, run 2). When the catalyst, following the thermal cycle above described, is recycled with no intermediate reduction, an increase of the activation energy for NO conversion is observed (Table 1, run 3). By contrast, when the catalyst is recycled with an intermediate reduction at 673 K, the low apparent activation energy initially observed is restored. Additionally, consecutive reductions decrease the activity of the catalyst (compare runs 1 and 4, Table 1). Metallic Rh atoms can be buried in the anionic array of the fluorite crystals (15), which may account for the decrease of activity.

The change of activation energy for NO conversion cannot be attributed to a change of selectivity from N_2O to N_2 on increasing the temperature since we did not observe strong variations of selectivity in N_2O in the various experiments. Moreover, also the activation energy for CO conversion is affected by the reduction at 673 K (Fig. 2.2).

The presence of two distinct activation energies for the NO–CO reaction was previously observed over Rh/Al_2O_3 catalysts and it was attributed to a shift of the rate limiting step (16, 17). Recent evidence (18), however, suggests that it can be associated with a variation of rhodium particle morphology due to CO-induced agglomeration/disruption processes involving the supported rhodium particles. Surface

TABLE 1

NO Reduction by CO over Rhodium Supported on $Ce_{0.6}Zr_{0.4}O_2$ and CeO_2: Reaction Rates and Activation Energies for NO and CO Conversions[a]

Run	CeO_2 (mol%)	Reduction temp. (K)	Rate[b] (mol NO converted g(catalyst)$^{-1}$s^{-1} × 10^8)	Activation energy (kJ mol^{-1})[c] (473–500 K) NO	(473–500 K) CO	(500–553 K) NO	(500–553 K) CO	(473–540 K) NO	(473–540 K) CO
1	60	473	4.1					125	130
2		673	3.7	65	100	146	147		
3[d]		—	0.6	117	92	146	142		
4[e]		673	1.3	75	96	138	142		
5	100	473	3.5					125	130
6		673	2.6					125	134

[a] Reaction conditions as reported in the Experimental section.
[b] Steady state reaction rates measured over catalysts aged at 473 K.
[c] Standard deviation ±8 kJ mol^{-1}.
[d] Catalyst recycled from run 2.
[e] Catalyst recycled from run 2.

OH groups promote the oxidative disruption process which results in a decrease of particle size according to the reaction shown in the following (19).

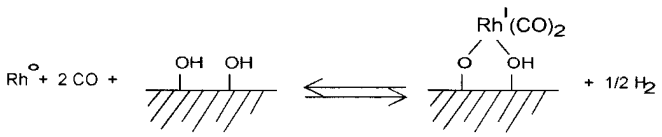

Therefore, a variation of particle size induced by agglomeration/disruption processes could be, in principle, responsible for the change of activation energy. However, due to the low surface areas of the present catalysts, a rather limited amount of surface OH should be available for the oxidative disruption, which is consistent with the observation of a single activation energy over both the Rh/CeO_2 and the $Rh/Ce_{0.6}Zr_{0.4}O_2$ reduced at 473 K. Consequently, the presence of two distinct activation energies for the $Rh/Ce_{0.6}Zr_{0.4}O_2$ reduced at 673 K needs an alternative explanation.

The reduced CeO_2 moieties show a powerful oxygen abstraction ability as they are easily reoxidized by a variety of oxygen-containing compounds such as CO_2 (14, 20), H_2O (20), and NO (21). Participation of the reduced $Ce_{0.6}Zr_{0.4}O_2$ in the NO conversion was therefore investigated in the absence of CO. As shown in Fig. 3.1, reduction at 473 K of $Rh/Ce_{0.6}Zr_{0.4}O_2$ does not promote a significant NO conversion. In contrast, a reduction at 673 K, results in a significant NO conversion. No oxygen was detected at the outlet of the reactor, suggesting that the NO conversion to give N_2 and N_2O occurs at the expense of a concomitant oxidation of the prereduced support.

Notably, the maximum rate of the NO conversion in the NO–CO reaction is 3.8×10^{-8} mol NO converted g_{cat}^{-1} s^{-1}, compared to the value of 3×10^{-7} mol NO converted g_{cat}^{-1} s^{-1} observed in the reaction of NO alone. The inhibiting effect of CO on the rate of NO conversion suggests that either CO can compete for the catalytic sites which are responsible for NO conversion or surface carbonates may form which hinder the ability of the support to reduce NO.

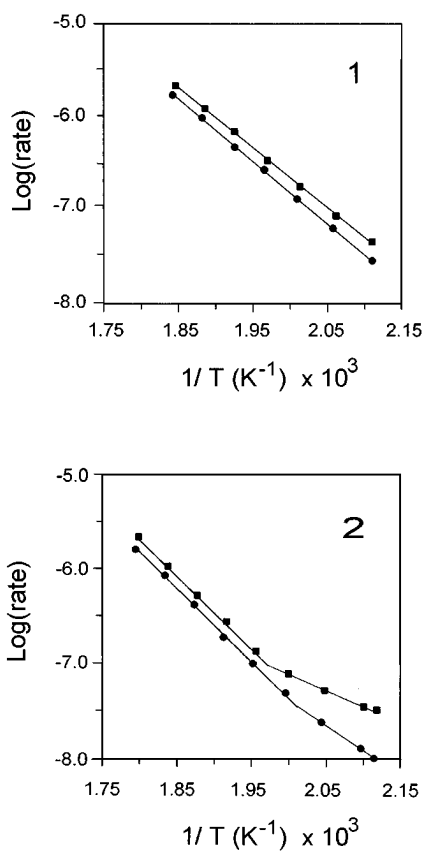

FIG. 2. Arrhenius plots for NO (■) and CO (●) conversions measured over 0.5% $Rh/Ce_{0.6}Zr_{0.4}O_2$, reduced at (1) 473 K and (2) 673 K.

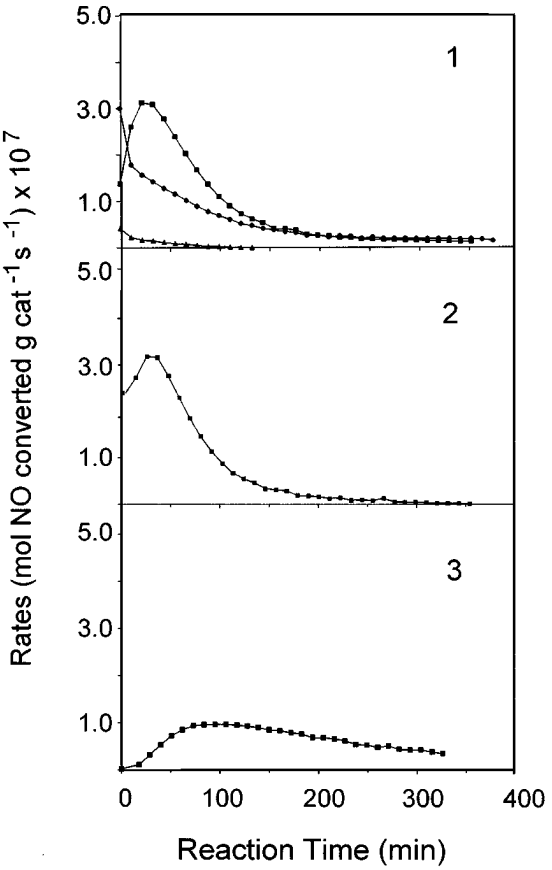

FIG. 3. Rate of conversion of NO at 473 K over (1) 0.5% $Rh/Ce_{0.6}Zr_{0.4}O_2$, reduced at 473 K (▲), reduced at 673 K (■), recycled and reduced at 673 K (●); (2) 0.5% $Pt/Ce_{0.6}Zr_{0.4}O_2$, reduced at 673 K; (3) $Ce_{0.6}Zr_{0.4}O_2$, reduced at 1073 K.

The primary role of the support in the conversion of NO is confirmed by the results shown in Figs. 3.2–3.3; both in the presence of Pt and even in the absence of the supported metal, NO is efficiently decomposed, provided that the $Ce_{0.6}Zr_{0.4}O_2$ solid solution has been reduced at a temperature sufficiently high to allow formation of bulk oxygen vacancies. Assuming a surface area of 1 $m^2\,g^{-1}$ and that only Ce^{3+} sites are present on the oxide surface, reoxidation of the surface of the support should require approximately 12 μmol of NO g_{cat}^{-1} (22). At an average rate of NO conversion of 0.25 μmol NO converted $g_{cat}^{-1}\,s^{-1}$, the surface of the support will be fully reoxidized after about 50 s of reaction. Therefore, the curves reported in Fig. 3 are associated with the reoxidation of the bulk of the support, since the first experimental point reported in Fig. 3 was sampled after 5 min of reaction.

Role of the Ce^{4+}/Ce^{3+} Redox Couple in the Conversion of NO: in situ XANES and Magnetic Susceptibility Measurements

Occurrence of a bulk redox process is evidenced by the XANES measurement (Fig. 4) which is a bulk-sensitive technique. The calcined $Rh/Ce_{0.5}Zr_{0.5}O_2$ sample (Fig. 4.1) shows a typical Ce L_{III} absorption edge of a pure Ce(IV) compound with three distinct lines denoted A, B_2, and C, respectively. With the resolution employed here, a structure B_1 appears as a shoulder on the intense B_2 line. Attribution of these lines has been discussed in detail elsewhere (23, 24 and References therein). By contrast, the Ce(III) state is characterized by a white line denoted B_0 which is observed, regardless of the nature of the Ce(III) compound. This line is shifted to higher energy by 1.85 eV from the B_1 line.

We do not find significant differences between the spectra of pure CeO_2 and that of calcined $Rh/Ce_{0.5}Zr_{0.5}O_2$ reported in Fig. 4.1. Small amounts of Ce^{3+} were observed for both Rh/CeO_2 (23) and Pd/CeO_2 (24) prepared from Cl-containing precursors and they were attributed to the formation of surface cerium oxychloride species which are thermally stable up to 723 K (25). The absence of Ce^{3+} can be attributed to the low surface area which prevents a strong interaction of the metal particles with the ceria–zirconia surface. Upon reduction of the calcined sample at 673 K (Fig. 4.2), the presence of the Ce^{3+} state is clearly detected by the appearance of the Ce^{3+} B_0 white line. Upon treatment of the reduced sample with a flow of NO at 473 K, the intensity of the B_0 line in the spectrum declines and features characteristic of the Ce(IV) state are again obtained

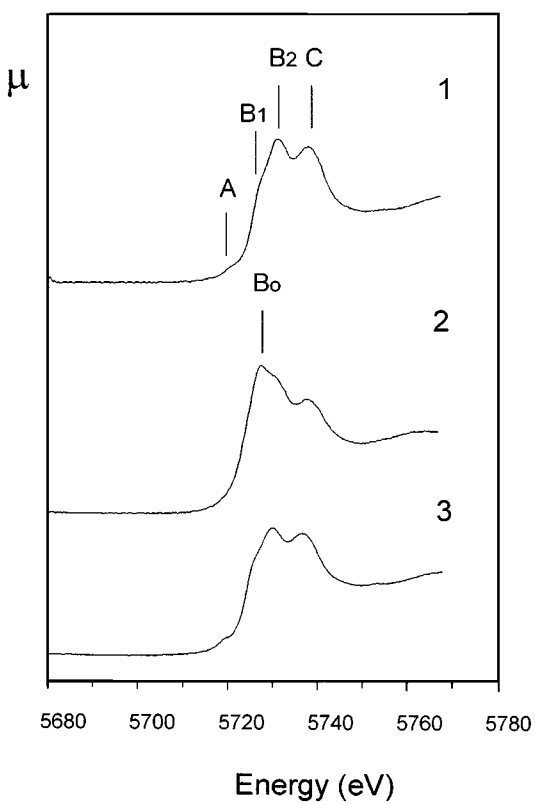

FIG. 4. *In situ* XANES spectra of cubic 0.5% $Rh/Ce_{0.5}Zr_{0.5}$ O_2: (1) as prepared; (2) reduced at 673 K, and (3) treated in diluted NO at 473 K.

(Fig. 4.3). This indicates that refilling the bulk oxygen vacancies occurs at the expense of a NO reduction process. Notably, no appreciable variation of the XANES spectrum measured at the K Zr edge could be detected in the same experiment which suggests that Zr takes no active role in the redox process.

Formation of Ce^{3+} after reduction at 673 K in the $Rh/Ce_{0.6}Zr_{0.4}O_2$ sample is confirmed by magnetic susceptibility measurements which showed a magnetic moment of 3.5×10^{-6} emu g^{-1} at 294 K. On the assumption that only Ce^{3+} is contributing to the magnetic moment, we estimate, according to Ref. 8, a composition of $Rh/Ce_{0.6}Zr_{0.4}O_{1.85}$ after the reduction at 673 K which is in fairly good agreement with that of $Rh/Ce_{0.6}Zr_{0.4}O_{1.88}$ obtained from the TPR experiment (compare Table 3). Upon treatment of this catalyst in a flow of diluted NO, we could not detect any measurable magnetic susceptibility, confirming the reoxidation of the support. The close correspondence between the degree of reduction as estimated from the magnetic susceptibility and TPR and the results of the XANES measurements indicates that the redox process occurs at the Ce sites.

Role of the Supported Metal in the Conversion of NO: NO Conversion and Temperature Programmed Oxidation Using NO as Oxidant over Reduced $M/Ce_{0.6}Zr_{0.4}O_2$ and $Ce_{0.6}Zr_{0.4}O_2$

The apparent activation energies for the conversion of NO were measured (Table 2) following the same scheme as employed in the NO–CO reaction. They fall in the range of activation energy observed for NO reduction in the NO–CO reaction over the $Rh/Ce_{0.6}Zr_{0.4}O_2$ reduced at 673 K. This suggests that, independently of the presence or nature of the supported metal, a common reaction pathway is responsible for the reduction of NO in the two reactions. It is not possible, however, to rule out some participation of the supported metal in the dissociation of NO in view of the different time dependence of the reaction rates reported in Figs. 3.1–3.3. The selectivity in formation of N_2O, which is the major product of the reaction at low temperatures (16), may give some insight into the role of the metal in the conversion of NO. Selectivity of 71% in N_2O is observed over the Rh-loaded sample reduced at 473 K (Table 2, run 1) which should be associated with NO dissociation occurring mainly on the Rh metal crystallites. At 473 K, reduction of the support should be limited essentially to the surface (5).

In the catalysts which were prereduced to create the oxygen vacancies in the bulk, the selectivity increases in the order: Rh < Pt < metal-free (Table 2, runs 2, 4, 6). This is consistent with the well-known ability of Rh to easily dissociate NO (26); however, the higher N_2O selectivity observed over the samples reduced at 673 K compared to that reduced at 473 K suggests a limited role of the metal in the NO dissociation process in the former case. High reduction temperature should favor rhodium particle sintering and it has been shown for Rh/Al_2O_3 catalysts (18) that increase of particle size favors NO dissociation and consequently N_2 formation.

A scanty role of the metal in the NO dissociation is further substantiated by TPO of the reduced catalysts using NO as oxidant (Fig. 5): the TPO of all the Rh, Pt, and metal-

TABLE 2

Conversion of NO over Supported and Unsupported $Ce_{0.6}Zr_{0.4}O_2$ Catalysts Reduced at Various Temperatures: Activation Energies and Selectivity in N_2O Formation[a]

Run	Metal	Reduction temp. (K)	Activation energy[b] (kJ mol^{-1})	N_2O selectivity (%)
1	Rh	473		71
2	Rh	673	67	89
3[c]	Rh	673		84
4	Pt	673	58	92
5[d]	Pt	673		87
6	—	1073	58	97

[a] Reaction conditions as reported in the Experimental section.

[b] Standard deviation ±8 kJ mol^{-1}, measured in the interval of temperatures 473–500 K.

[c] Catalyst recycled from run 2.

[d] Catalyst recycled from run 4.

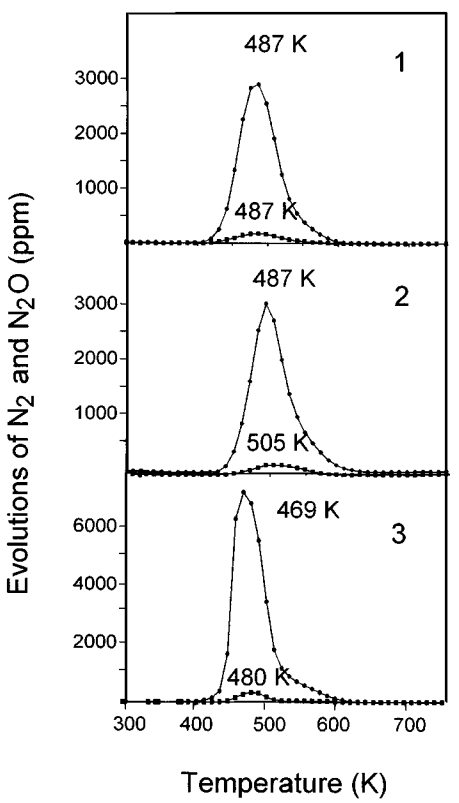

FIG. 5. Temperature programmed oxidation by NO: N_2 (■) and N_2O (●) evolution: (1) 0.5% $Rh/Ce_{0.6}Zr_{0.4}O_2$, reduced at 673 K; (2) 0.5% $Pt/Ce_{0.6}Zr_{0.4}O_2$, reduced at 673 K; (3) $Ce_{0.6}Zr_{0.4}O_2$, reduced at 1073 K.

TABLE 3

Conversion of NO over Supported and Unsupported $Ce_{0.6}Zr_{0.4}O_2$ Catalysts Reduced at Various Temperatures

Run	Metal	Reduction temperature[a] (K)	H_2 consumption[b] (ml g^{-1})	Equivalent O_2 release[c] (ml g^{-1})	O_2 uptake[d] (ml g^{-1})
1	Rh	673	17.5	8.8	10.7
2[e]	Rh	673			10.7
3	Pt	673	20.6	10.3	10.9
4[f]	Pt	673			9.7
5	—	1073	8.2	4.1	17.9

[a] Reduction time 2 h, starting from r.t., heating rate 10 K min^{-1}.
[b] ±1–2 ml H_2 g^{-1}, measured during reduction in H_2 (5%) in Ar.
[c] Calculated from the H_2 consumption.
[d] Calculated from the NO conversion experiment, ±2 ml O_2 g^{-1}; reduction carried out in pure H_2.
[e] Catalyst recycled from run 1.
[f] Catalyst recycled from run 3.

free catalysts shows a single broad feature for N_2O and N_2 evolution centered at 470–505 K.

The H_2 consumption and the oxygen uptake measured in the NO conversion experiments are summarized in Table 3. The Rh- and Pt-loaded samples show a high capacity to exchange oxygen. The comparable values of H_2 and O_2, as measured from the reduction and NO conversion, are in agreement with the occurrence of NO conversion at the expense of support reoxidation. The values measured for $Ce_{0.6}Zr_{0.4}O_2$ deserve some comments: the high value of O_2 uptake and the low value of H_2 consumption are attributed to the different conditions employed in the reduction in the TPR equipment and in the flow reactor (5% H_2 in Ar and pure H_2 were employed, respectively). In the presence of the supported metal, H_2 activation is highly efficient (compare Fig. 1) and therefore comparable values are obtained. In its absence, H_2 activation on the support is difficult and therefore use of pure H_2 significantly increases the degree of reduction as compared to the TPR experiment. Consequently, the O_2 uptake over the unsupported sample is about twice that of the Rh- and Pt-loaded samples.

Examination of Fig. 5 reveals that there are some shifts in the peak temperatures, reoxidation of the unsupported sample being favored, compared to the metal-loaded samples. Formation of Ce^{3+} upon reduction expands the lattice of the CeO_2–ZrO_2 solid solution (10) giving a more open structure favoring the oxidation of the reduced sample.

Selectivities in N_2O formation of 94, 95 and 94% were measured in the TPO respectively for the Rh, Pt, and metal-free catalyst, suggesting a unique driving force for the dissociation of NO. Significantly, a Rh/Al_2O_3 catalyst did not show any measurable N_2 and N_2O formation in the same experiment. This observation strongly suggests that the driving force for the dissociation of NO is provided by the presence of bulk oxygen vacancies formed in the reduction of the support.

An important role of surface oxygen vacancies or surface oxygen nests (17) in determining the catalytic behavior of M/CeO_2 systems has been emphasized several times (2, 13, 14, 27). The oxygen vacancies associated with reduced ceria in the proximity of noble metal particles have been suggested as promoting sites for NO and CO conversions (13, 27), while only recently long-range effects involving bulk CeO_2 lattice oxygen are being recognized to play an important role in these phenomena. Thus, CO TPD from a Rh/CeO_2 catalyst showed that migration of lattice oxygen from CeO_2 to the metal occurs (28).

The OSC was increased by formation of a La_2O_3–CeO_2 solid solution in Pt, Rh/La_2O_3–CeO_2/Al_2O_3 catalysts which was attributed to the formation of lattice oxygen vacancies due to La^{3+} incorporation (29).

Serre *et al.* (30) have recently observed an enhancement of the rate of CO oxidation over reduced Pt/CeO_2 catalysts which was attributed to the presence of bulk oxygen vacancies. Participation of lattice oxygen has been recognized in several oxidation reactions while the present results suggest that the bulk oxygen vacancies play an important role in promoting the rate of the oxygen exchange reactions also in a reduction process.

The strong similarities in the TPO behavior between metal-loaded and metal-free samples strongly suggest that the activation of NO occurs mainly on the oxide surface. It has been shown that NO chemisorbs strongly on pure CeO_2 (31). At low temperatures we could not detect any NO dissociation, i.e., N_2O and N_2 formation, since the surface oxygen vacancies initially present are immediately annihilated. Upon increasing the temperature, the oxygen migration in the bulk is promoted and a vacancy concentration gradient is established, providing the driving force for the dissociation of the adsorbed NO. The participation of the metal or of the metal-support interface to the NO dissociation appears limited, while their role in enhancing the CO

oxidation rates has been established. Recently, Zafiris and Gorte (32) found evidence for an important role of oxygen migration from CeO_2 to Rh in enhancing the activity of Rh/CeO_2 catalyst in CO oxidation. Such an oxygen migration will provide the way to regenerate the availability of support oxygen vacancies for NO dissociation forming a catalytic cycle such as that depicted in the following.

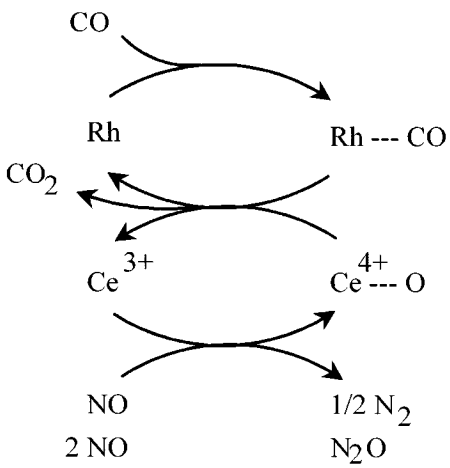

Above 500 K, the oxygen mobility is high enough to allow annihilation of all bulk oxygen vacancies, which destroys the vacancy concentration gradient. No dissociation of NO occurs over the reoxidized support and therefore we measure an activation energy of 125 kJ mol^{-1} for NO conversion, which is associated with a metal-catalyzed cycle.

The effects of recycling on the activity of the $Rh/Ce_{0.6}Zr_{0.4}O_2$ catalyst is another point worthy of discussion. The attribution of the inhibition period observed in the decomposition of NO (Fig. 3.1) to a reoxidation of Rh atoms buried in the fluorite lattice (23) should be discharged. By recycling the catalyst with an intermediate reduction, the inhibition should still be present. On the contrary, when the reduction/reoxidation cycles are repeated, the catalyst becomes more prompt to sustain the redox cycle and the inhibition period is no longer observed. Our previous investigation (5) has shown that the rate of the bulk reduction process is related to the structural properties and particularly to the presence of structural defects. Upon reduction of CeO_2, a strong expansion of the lattice is observed due to the larger Ce^{3+} (0.11 nm) ionic radius compared to that of Ce^{4+} (0.097 nm) and subsequent reoxidation shrinks the lattice parameter (23). It appears reasonable that upon repeating the redox cycles, the stress due to these continuous changes of the lattice parameter may easily induce formation of structural defects, promoting oxygen mobility in the framework. The oxygen mobility is rate-limiting the redox processes in the bulk, Higher mobility will therefore result in an increase of the initial rate of the bulk reoxidation. This is a rather important observation since the OSC of CeO_2 is generally associated with surface redox processes (2, 27, 33).

Favorable effects of reduction of CeO_2 on the CO conversion activity of a $Pt–CeO_2$ containing TWC increased as the mean particle size of CeO_2 decreased from 100 nm to 6.7 nm (13). The reduction of CeO_2 is promoted upon decreasing the particle size and therefore formation of bulk oxygen vacancies is favored. We observed in the course of TPO experiments carried out on samples of Rh/CeO_2 of high surface area that reoxidation of the surface by NO occurs even at r.t. which suggests that surface oxygen vacancies should be immediately annihilated in the reaction conditions.

Recently, it has been found (34) that the strong enhancement of CO_2 hydrogenation observed after a reduction at 773 K of a Rh/CeO_2 catalyst (14) is strongly dependent on the crystallite size of the CeO_2. Over $Rh/CeO_2–SiO_2$ catalysts, this effect is no longer observed for particle size below 8 nm, since CeO_2 appeared to be spread over the SiO_2 surface and no crystalline CeO_2 phase was detected. All these observations are consistent with the role of bulk oxygen vacancies in enhancing the activity of CeO_2-based catalysts. Significantly, Padeste and Baiker observed that an air pulse brings a TWC into an oxidized state which reduces the NO_x and hydrocarbon conversions and only after a reduction by a rich exhaust was good efficiency again attained (35). Therefore, in view of the above discussion, the strong promotion of the bulk redox processes in the metal-loaded $CeO_2–ZrO_2$ solid solutions compared to Rh/CeO_2 makes these materials of strong interest for automotive applications, since bulk Ce(IV) sites might become easily available for redox processes even in transient conditions.

CONCLUSIONS

The results presented here clearly indicate an important role of bulk oxygen vacancies in promoting NO conversion over metal-loaded $CeO_2–ZrO_2$ catalysts. An oxygen vacancy gradient is indicated as the driving force for NO dissociation, suggesting that it may be responsible for the enhanced NO and CO conversions previously observed over reduced M/CeO_2 catalysts (2, 12, 22, 23). XANES measurements show that the Ce^{4+}/Ce^{3+} redox couple directly interacts with NO, favoring its reduction over the Ce^{3+} sites to give N_2 and N_2O. ZrO_2 does not take an active role in the NO conversion whereas it is responsible for the enhancement of the oxygen mobility in the bulk (5). This results in an easy formation of bulk oxygen vacancies. However, the activation of the reducing agent is difficult on the bare support and the presence of the metal is necessary to activate and spill it over to the support.

ACKNOWLEDGMENTS

Dr. Francoise Villain (LURE, Orsay, France) is acknowledged for assistance during the XANES measurements. Mr. Elvio Merlach and Mr. Renzo Crevatin (Dipartimento di Scienze Chimiche, Università di

Trieste) are acknowledged for the design and construction of the *in situ* XANES cell. Dr. Roberta Sessoli (Dipartimento di Chimica, Università di Firenze) is acknowledged for the magnetic susceptibility measurements The Consiglio Nazionale delle Ricerche (Rome), the Ministero dell'Università e della Ricerca Scientifica (Rome), Università di Trieste, and Magneti Marelli D.S.S. are acknowledged for financial support.

REFERENCES

1. Taylor, K. C., *in* "Catalysis-Science and Technology" (J. R. Anderson and M. Boudart, Eds.), Vol. 5. Springer-Verlag, Berlin, 1984.
2. Harrison, B., Diwell, A. F., and Hallett, C., *Platinum Met. Rev.* **32**, 73 (1988).
3. Shyu, J. Z., Weber, W. H., and Gandhi, H. S., *J. Phys. Chem.* **92**, 73 (1988).
4. Harkonen, M. A., Aitta, E., Lahti, A., Luoma, M., and Maunula, T., *SAE Technical Paper* 910846, 1991.
5. Fornasiero, P., Di Monte, R., Ranga Rao, G., Kašpar, J., Meriani, S., Trovarelli, A., and Graziani, M., *J. Catal.* **151**, 168 (1995).
6. Hecker, W. C., and Bell, A. T., *J. Catal.* **84**, 200 (1983); Cho, B. K., Shanks, B. H., and Bailey, J. E., *J. Catal.* **115**, 486 (1989).
7. Ranga Rao, G., Kašpar, J., Meriani, S., Di Monte, R., and Graziani, M., *Catal. Lett.* **24**, 107 (1994).
8. Laachir, A., Perrichon, V., Badri, A., Lamotte, J., Catherine, E., Lavalley, J. C., El Fallah, J., Hilaire, L., Le Normand, F., Quemere, E., Sauvion, N. S., and Touret, O., *J. Chem. Soc. Faraday Trans.* **87**, 1601 (1991).
9. McHale, A. E., "Phase Diagrams for Ceramists," Annual 1991, p. 20.
10. (a) Meriani, S., *Mat. Sci. Eng.* **71**, 369 (1985); (b) Meriani, S., and Spinolo, G., *Powder Diffraction* **2**, 255 (1987); (c) Meriani, S., *Mater. Sci. Eng. A* **109**, 121 (1989).
11. Yashima, M., Morimoto, K., Ishizawa, N., and Yoshimura, M., *J. Amer. Ceram. Soc.* **76**, 1745 (1993).
12. Nunan, J. G., Robota, H. J., Cohn, M. J., and Bradley, S. A., *J. Catal.* **133**, 309 (1992).
13. Yao, H. C., and Yu Yao, Y. F., *J. Catal.* **87**, 152 (1984).
14. Trovarelli, A., Dolcetti, G., de Leitenburg, C., Kašpar, J., Finetti, P., and Santoni, A., *J. Chem. Soc. Faraday Trans.* **88**, 1311 (1992).
15. Sanchez, M. G., and Gazquez, J. L., *J. Catal.* **104**, 120 (1987).
16. Hecker, W. C., and Bell, A. T., *J. Catal.* **85**, 389 (1984).
17. Oh, S. H., *J. Catal.* **124**, 477 (1990); Oh, S. H., and Eickel, C. C., *J. Catal.* **128**, 526 (1990).
18. Kašpar, J., de Leitenburg, C., Fornasiero, P., Trovarelli, A., and Graziani, M., *J. Catal.* **146**, 136 (1994).
19. Smith, A. K., Hughes, F., Théolier, A., Basset, J. M., Ugo, R., Zanderighi, G. M., Bilhou, G. M., Bilhou-Bougnol, V., and Graydon, V. F., *Inorg. Chem.* **18**, 3104 (1979); Solymosi, F., and Pasztor, M., *J. Phys. Chem.* **89**, 4789 (1985).
20. Otsuka, K., Hatano, M., and Morikawa, A., *J. Catal.* **79**, 493 (1983).
21. Hertz, R. K., *Ind. Eng. Chem. Prod. Res. Dev.* **20**, 451 (1981).
22. Perrichon, V., Laachir, A., Bergeret, G., Fréty, R., and Tournayan, L., *J. Chem. Soc. Faraday Trans.* **90**, 773 (1994).
23. El Fallah, J., Boujana, S., Dexpert, H., Kiennemann, A., Majerus, J., Touret, O., Villain, F., and Le Normand, F., *J. Phys. Chem.* **98**, 5522 (1994).
24. Le Normand, F., Hilaire, L., Kili, K., Krill, G., and Maire, G., *J. Phys. Chem.* **92**, 2561 (1988).
25. Klevtzov, P. C. R., *Acad. Sci. Ser. C* **266**, 385 (1966).
26. Root, T. W., Schmidt, L. W., and Fisher, G. B., *Surf. Sci.* **134**, 30 (1983).
27. Diwell, A. F., Rajaram, R. R., Shaw, H. A., and Truex, T. J., *in* "Catalysis and Automotive Pollution Control II," *Stud. Surf. Sci. Catal.* (A. Crucq, Ed.), Vol. 71, p. 139. Elsevier, Amsterdam, 1991; Munuera, G., Fernandez, A., and Gonzalez-Elipe, A. R., *Stud. Surf. Sci. Catal.* (A. Crucq, Ed.), Vol. 71, p. 207. Elsevier, Amsterdam, 1991.
28. Jin, T., Okuhara, T., Mains, G. J., and White, J. M., *J. Phys. Chem.* **91**, 3310 (1987).
29. Miki, T., Ogawa, T., Haneda, M., Kakuta, N., Ueno, A., Tateishi, S., Matsura, S., and Sato, M., *J. Phys. Chem.* **94**, 644 (1990).
30. Serre, C., Garin, F., Belot, G., and Maire, G., *J. Catal.* **141**, 9 (1993).
31. Niwa, M., Furukawa, Y., and Murakami, Y., *J. Coll. Interface Sci.* **86**, 260 (1982).
32. Zafiris, G. S., and Gorte, J., *J. Catal.* **143**, 86 (1993).
33. Belton, D. N., and Schmieg, S. J., *J. Vac. Sci. Technol. A* **11**, 2330 (1993).
34. Trovarelli, A., de Leitenburg, C., Dolcetti, G., and Lorca, J. L., *J. Catal.* **151**, 111 (1995).
35. Padeste, L., and Baiker, A., *Ind. Eng. Chem. Res.* **33**, 1113 (1994).